Proceedings of ASME Turbo Expo 2024
Turbomachinery Technical Conference and Exposition
GT2024
June 24-28, 2024, London, United Kingdom

GT2024-127151

DRAFT: COMPRESSOR BLADE VIBRATIONS OF NEXT GENERATION OF TURBOCHARGER WITH FOCUS ON DAMPING: SIMPLIFIED PREDICTION AND AI-BASED EVALUATION

Robby Weber*, Matthias Glatt

Accelleron, Turbo Systems Switzerland Ltd., Baden, Switzerland

ABSTRACT

Recently, Accelleron launched the X300-L series [1], marking the beginning of a new era in turbocharger technology. This innovative platform-based approach simplifies service procedures but also provides adaptability to respond to diverse demands caused by a certain variety of future fuels. The integration of enhanced power densities, standardized components, and a modular design results in a decrease in frame sizes and variants. Consequently, individual core components (i.e., compressor wheel or turbine impeller) are necessarily not only more compact and more powerful but also extend their utility across a wider range of applications.

Accurate blade vibration analysis is essential to identify potential performance issues, mitigate fatigue and wear, and prevent disastrous failures. The scope of numerical and experimental methods that are involved during the modern development process of new turbochargers will easily extend the scope of a single contribution. To allow a more detailed insight, this paper presents a comprehensive study on compressor blade vibrations - with a particular focus on damping as one of the most important aspects of high-cycle fatigue.

First, a simplified method is adopted to predict critical damping ratios of specific blade vibration resonances. This approach incorporates inputs as modal parameters (like natural frequency and mode shape) and operational conditions (fluid density and speed of sound), all of which are conveniently accessible during the preliminary design phase.

Second, a blade vibration measurement is carried out employing both strain gauges and blade tip timing, two cutting-edge methodologies that demonstrate exceptional mutual consistency. The dynamic stress of five chosen resonance crossings is investigated to primarily underline the robustness against high-cycle fatigue and show the agreement between strain gauge and tip timing measurements.

Third, experimental data from several resonance crossings recorded with strain gauges are fed into an AI-driven methodology utilizing Deep Learning, enabling the assessment of genuine damping ratios for these resonances. Subsequently, a comparison is presented, contrasting the new damping evaluation (AI based on strain gauge measurement) with a state-of-the-art solution (SDOF-Fit of tip timing data) as well as the predicted damping ratios of the first part.

In conclusion, this paper not only highlights the exceptional performance of the compressor but also underscores its accelerated development through the use of reliable data from the early design phase. Modern measurement techniques offer a remarkable precision that allows a high trust in numerical methods. The proposed method offers practical tools for engineers in the field, facilitating the development of more reliable and efficient turbocharging systems for future applications.

Keywords: Radial Compressor, Blade Vibration, Damping, BTT, SG, AI, Neural Network

NOMENCLATURE

Abbreviations

BTT	Blade Tip Timing
FE	Finite Element
HCF	High-Cycle Fatigue
LSMF	Least Square Model Fit
MDOF	Multi-Degree-of-Freedom
ND	Nodal Diameter
SDOF	Single-Degree-of-Freedom
SG	Strain Gauge

Roman Letters

a_{Blade}	Orthogonal Distance Between 2 Blades [mm]
c	Speed of Sound [mm/s]
EO	Engine Order [-]
f	Frequency [Hz]
$\boldsymbol{n}$	Surface Normal Vector [mm]
n	Mech. Speed [rps]
p	Pressure [Pa]
R_s	Specific Gas Constant [J kg^{-1} K^{-1}]
r	Radius [mm]

*Corresponding author: robby.weber@accelleron-industries.com

T	Temperature [K]
t	Time [s]
u	Displacement [mm]

Greek Letters

ζ	Damping Ratio [-]
Θ	Probes Circumferential Position [°]
κ	Adiabatic Index [-]
λ	Wave Length [mm]
ξ	Acoustic Criteria [-]
ρ	Fluid Density [kg/mm^3]
σ	Mech. Stress [MPa]
$\boldsymbol{\varphi}$	Natural Mode Shape $\left[\sqrt{\frac{mm}{kg}}\right]$
ω	Natural Angular Frequency $\left[\frac{1}{s}\right]$

Subscripts

exp	expected
k	k-th Cell
m	m-th Mode
meas	measured
res	Resonance
TC	Turbo Charger

INTRODUCTION

Radial turbines and compressor wheels are the most important components of turbochargers, which greatly enhance the performance of modern internal combustion engines across a wide range of applications. Developments are seeking answers to new questions. Today, in a certain ecological reorientation of the market, core components must not only work more efficiently in smaller frame sizes but also be able to respond to rather short-term changes (e.g., various fuel alternatives [2]) despite decades of usage. The basic trend continues towards higher efficiencies, higher pressure ratios, and higher flow capacity. This requires thinner blade thicknesses, longer blades, and slimmer geometries in the design. Each of these changes has a direct (and mostly detrimental) effect on the resistance to high-cycle fatigue. Blade vibrations represent one of the most important topics in the field of HCF strength.

In an industrial environment, design and testing are very closely linked to each other. As a principle, a new component or a new product must successfully pass several qualification tests before it goes into series production. One of the more complex tests is dedicated to the experimental investigation of blade vibrations. These are measured either by contact using strain gauges or non-contact by tip timing system or a combination of both. For preliminary resonance identification, relevant natural modes can also be visualized by a surface scan with LDV [3–5]. Recently, resonance crossings form of a small turbocharger in test operation were captured by a high-speed camera [6].

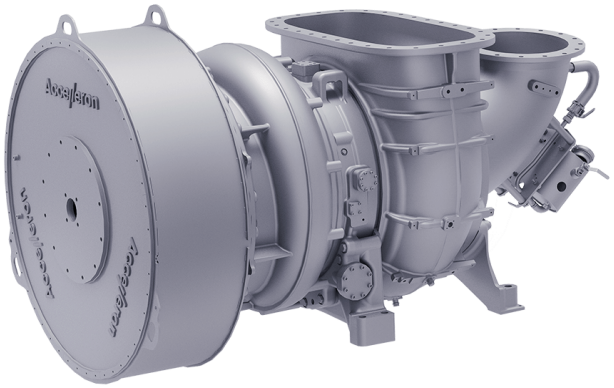

FIGURE 1: NEXT GENERATION TURBOCHARGER ACCX300-L

Research in recent decades has focused heavily on the topics of mistuning and damping [7, 8], the prediction of vibrational stress due to blade vibrations in operation [9], and even intentional blade mistuning with the aim of reducing blade vibration amplitudes [10–12]. The constantly evolving simulations benefit from both super-fine FE models, which depict the smallest manufacturing inaccuracies [13, 14], and from reduced order models [15], which depict the random character of blade mistuning and quantify their effects in terms of an amplifications in a very short time with heavily reduced computational effort.

The design process usually involves a very intensive evaluation of different design approaches according to various criteria (e.g., thermodynamic performance, safety against HCF, etc.). Especially in the early phase - particularly without available hardware and qualification tests - simulations are the only options to move further. In the highly complex field of blade vibrations, the reliable prediction of excitation forces and damping are the key topics for reliable statements based on FE models [16]. For damping ratios, Beirow et al. [17, 18] contributed with an approach to quantify them based on stationary operation data and modal information. The method was validated using an axial high-pressure compressor stage initially at standstill and then at operational conditions. Weber [19] transferred the method to radial compressors and turbines of various sizes at a standstill. Nakos et al. [20] further improved the method with a valid application on fundamental natural modes. With a certain discrepancy between prediction and measurement evaluation, Spengler et al. [16] already employed this method during the design of a radial turbine impeller.

This paper aims to close the remaining gap in the damping of a radial compressor wheel during operation. The method is shown in a single operation point and selected resonance crossings. This paper consists of 4 sections. First, the formula for calculating damping ratios due to acoustic emissions is introduced. In the following section, the measurement setup of the compressor blade vibration measurement is presented. Then, the concept of an artificial intelligence blade vibration analysis method (AIBVAM) is presented and employed to determine damping ratios from strain gauge data. In the final section, the results are brought together and critically compared with each other. The paper concludes with an outlook on the next steps for the further development of AI-based evaluations.

DAMPING PREDICTION

Generally, damping is a superposition from different sources, e.g. junctions, inner material, bearings, and fluid interaction. In the frame of turbomachinery with a focus on blade vibrations of integrally manufactured components, the mechanisms may be simplified to damping due to fluid interaction and may benefit from inner material damping. Maywald et al. [21] proves a fundamental relation between fluid density ρ and damping ratio ζ in both a standstill and operating conditions. As shown in Fig 2, the critical damping ratio linearly increases with the fluid density. Usually, there is a small (but positive) offset of damping if fluid density reaches an insignificant level (i.e. technical vacuum). This portion is usually known as inner material damping.

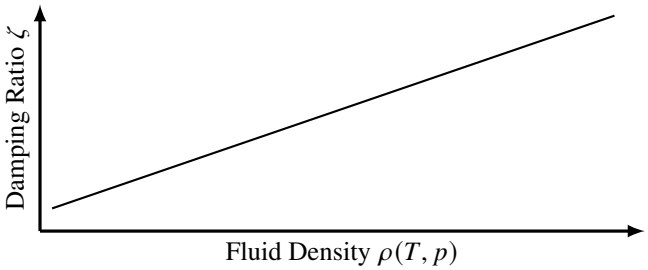

FIGURE 2: LINEAR CORRELATION BETWEEN MODAL DAMPING AND FLUID DENSITY

Based on this finding, the same working group [17, 18] published an approach and a validation of a simplified method to predict the fluid-induced damping from acoustic emissions. For higher modes (i.e. the acoustic wave does not reflect on neighboring blades), the damping ratio of a resonance mode m is determined using

$$\zeta_m = \frac{1}{2\omega_m} \sum_k \rho_k \cdot c_k \cdot \boldsymbol{\varphi}_{m,k}^T \left(\boldsymbol{\varphi}_{m,k} \cdot \boldsymbol{n}_k\right) \frac{\boldsymbol{n}_k}{|\boldsymbol{n}_k|}. \tag{1}$$

This formula incorporates the following inputs from FE calculation ω_m as a resonance mode m's natural angular frequency, $\boldsymbol{\varphi}_{m,k}$ as the corresponding mode shape vector of each surface element k and the normal surface vector $\boldsymbol{n}_k$ of this element. Further from stationary fluid dynamics, the cell's fluid density ρ_k and speed of sound c_k affect the damping ratio. For the frame of this paper, a single operation point (namely Design Point in Fig. 4) is considered. Therefore the damping evaluation is focussed on resonances that are excited close to this point.

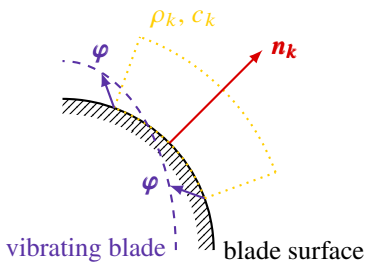

FIGURE 3: SCHEMATIC BLADE SURFACE, MODAL DISPLACEMENT AND ADJACENT FLUID CELL (IDEA FROM BEIROW ET AL. [17])

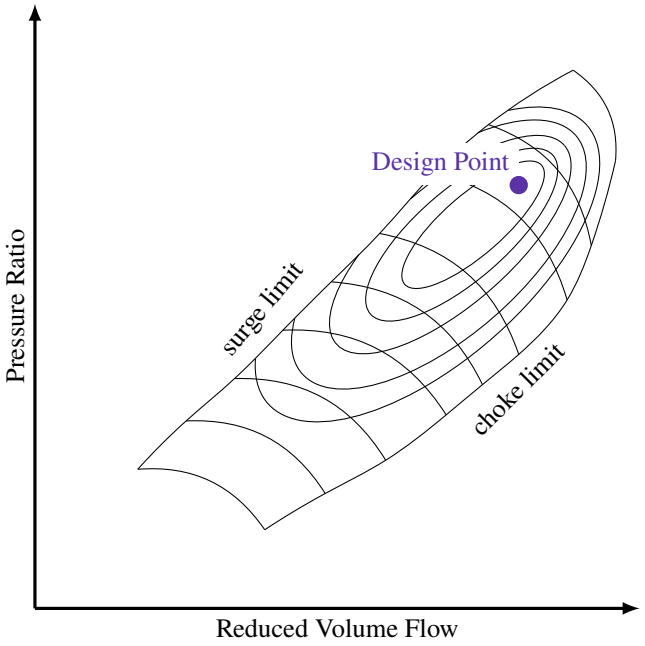

FIGURE 4: SCHEMATIC COMPRESSOR MAP OF A RADIAL COMPRESSOR WHEEL

Based on previously existing measurement data from radial turbine impellers and compressor wheels in different sizes [19], Nakos et al. [20] performed a rather empirical study and extended the formula for fundamental modes, whose radiated acoustic waves interact with neighboring blades. χ is introduced to serve as a frequency- and temperature-dependent acoustic criteria to differentiate between fundamental or high modes:

$$\chi = \frac{\lambda}{a_{blade}} = \frac{c}{f \cdot a_{blade}} = \frac{\sqrt{\kappa R_s T}}{f \cdot a_{blade}} \tag{2}$$

For fundamental modes $\chi > 1.5$, the computed damping ratio in eqn. 1 is additionally divided by χ:

$$\zeta_m = \begin{cases} \dfrac{1}{2\omega_m} \sum \rho_k \cdot c_k \cdot \boldsymbol{\varphi}_{m,k}^T \left(\boldsymbol{\varphi}_{m,k} \cdot \boldsymbol{n}_k\right) \dfrac{\boldsymbol{n}_k}{|\boldsymbol{n}_k|} & \chi < 1.5 \\ \dfrac{1}{2\omega_m} \sum \dfrac{\rho_k \cdot c_k}{\chi} \cdot \boldsymbol{\varphi}_{m,k}^T \left(\boldsymbol{\varphi}_{m,k} \cdot \boldsymbol{n}_k\right) \dfrac{\boldsymbol{n}_k}{|\boldsymbol{n}_k|} & \chi > 1.5 \end{cases} \tag{3}$$

The determination of a_{blade} as the (shortest) orthogonal distance between two neighboring blades requires some additional attention in the use case of radial compressor wheels since they usually have main and splitter blades. Figure 5 shows the predicted damping ratios according to Eq. 3. Please note that the thermodynamic inputs are derived from a single operation point (see Fig. 4). Only a few resonances are actually linked to that point.

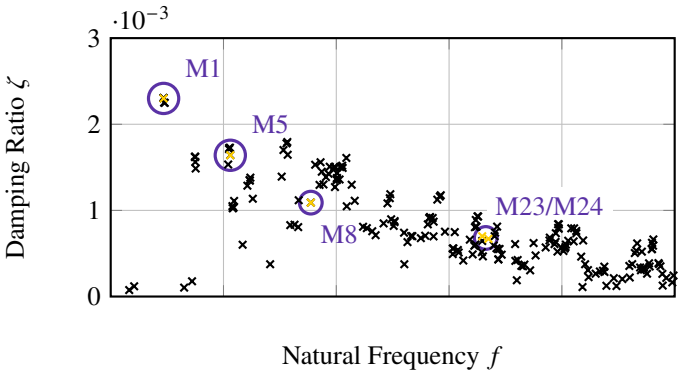

FIGURE 5: PREDICTED DAMPING RATIO OF A RADIAL COMPRESSOR

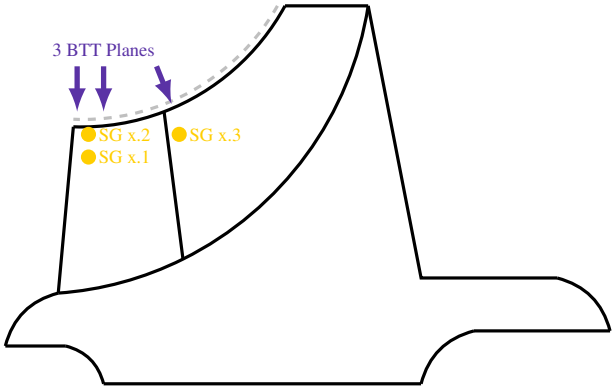

FIGURE 7: SCHEMATIC INDICATION OF MEASUREMENT POINTS (STRAIN GAUGE AND BLADE TIP TIMING)

MEASUREMENT SETUP

In the scope of this paper, 5 synchronous resonance crossings are investigated, namely M1, M5, M8, M23, and M24. Their positions are shown in the Campbell Diagram in Fig. 6. M23 and M24 are excited from the same engine order, so 4 different engine orders excite those resonances of interest. The different sources of excitation are caused by inhomogeneities in the inflow distribution (low engine order excitation), and single and double count of downstream stator vanes (high engine order excitation).

The displacements (i.e., their mode shapes $\boldsymbol{\varphi}$, see Appendix A) and consequently the stress and strain field of those resonance crossings differ dramatically from mode to mode. For reliable analysis of all resonances, several measurement positions are used. Furthermore, both strain gauge (SG) and blade tip timing measurements (BTT) are done in parallel to maximize the data obtained from a single run. The measurement positions are shown on a simplified compressor in Fig. 7.

There are 3 different SG positions, two of them on the main blade and one on the splitter blade. 4 main and splitter blades are equipped with SGs for this measurement. So in total, 12 SGs are recording the strains due to blade vibrations. Supplementary, there are 24 blade tip timing probes in the casing, that observe the blade vibrations at three different axial planes of every blade simultaneously. Figure 8 depicts a subset of the probes within the compressor casing.

The sampling rate of SGs is usually free to choose. More likely, a restriction may come from the telemetry transmission system. In most cases, the sampling rate easily exceeds the Nyquist theorem of relevant blade vibration frequencies. A rough workflow may consist of a truncation into smaller sample sizes (approx. 40ms), a Fourier-Transformation, and an assignment to engine orders. Finally, the strain spectrum is transformed into a physical value that allows a human evaluation against HCF, for example, material utilization, af-strength, or stress.

Usually, blade vibration analysis using tip timing is more complex and time-consuming than SG analysis. However, the basic idea to derive vibration amplitude from time of arrival (ToA) allows a non-intrusive measurement of all blades at the same time with usually less effort in preparation for blade vibration testing. From the difference time Δt between the expected time of arrival t_{exp} without blade vibration and the actual measured time of arrival t_{meas} with blade vibration:

$$\Delta t = t_{exp} - t_{meas} \tag{4}$$

the corresponding blade deflection u is directly computed if the rotor speed n_{TC} and radial position r are known:

$$u = \Delta t \cdot n_{TC} \cdot r \tag{5}$$

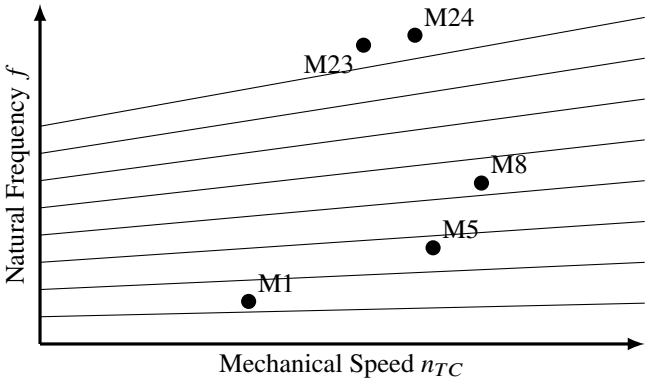

FIGURE 6: SCHEMATIC CAMPBELL DIAGRAM OF A RADIAL COMPRESSOR WHEEL WITH RESONANCE CROSSINGS

FIGURE 8: TYPICAL APPLICATION OF BLADE TIP TIMING PROBES IN A COMPRESSOR CASING

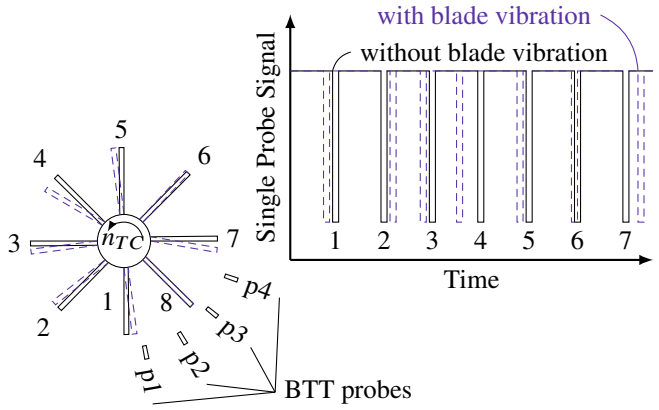

FIGURE 9: THE PRINCIPLE OF BLADE TIP TIMING

Even if BTT measurements are done employing optical probes, a certain noise in the data is unavoidable. That prevents an instantaneous determination of vibration stress based on blade deflection. Further, a direct Fourier transformation is not meaningful due to aliasing effects related to a low sampling frequency. A circumferential least square model fit (LSMF, Eq.6) [22] of the blade's amplitude during a single revolution at the probes circumferential position Θ is widely used to determine resonance amplitude and frequency based on a valid guess of the engine order EO.

$$\begin{bmatrix} u_{p1} \\ \vdots \\ u_{p4} \end{bmatrix} = \begin{bmatrix} 1 & \cos(EO \cdot \Theta_{p1}) & \sin(EO \cdot \Theta_{p1}) \\ \vdots & \vdots & \vdots \\ 1 & \cos(EO \cdot \Theta_{p4}) & \sin(EO \cdot \Theta_{p4}) \end{bmatrix} \cdot \begin{bmatrix} a_0 \\ a_1 \\ a_2 \end{bmatrix} \tag{6}$$

From the measured displacements $u_{p1} \cdots u_{p4}$, the vibration amplitude $A = \sqrt{a_1^2 + a_2^2}$ can be determined for every revolution. A linear transmission factor converts this amplitude into dynamic stress σ, see Fig. 15 and 16.

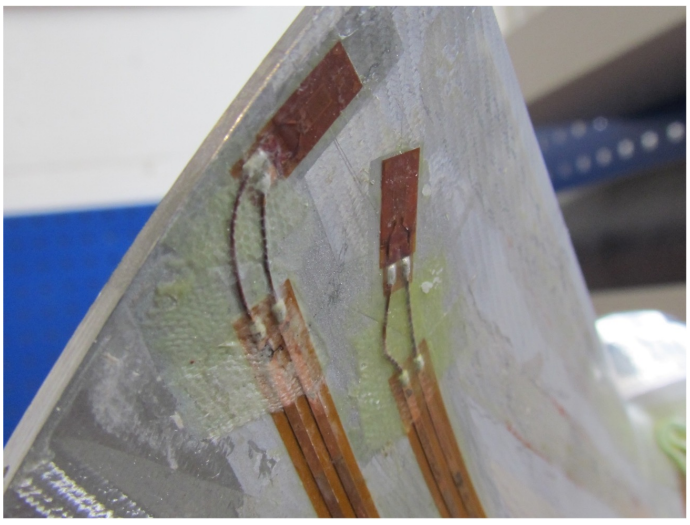

FIGURE 10: TYPICAL APPLICATION OF STRAIN GAUGES ON A COMPRESSOR BLADE

AI-BASED DAMPING EVALUATION

Damping ratios for resonance crossings measured on turbocharger compressors or turbine blades, e.g. with strain gauges, generally can be determined by fitting a simple Single-Degree-of-Freedom (SDOF) model to the measured data. The model's parameters are determined so that the amplitude (and/or phase) trend over frequency calculated by the SDOF model fits best to the measured resonance data. The damping factor is obtained as one of the model's parameters.

For a single blade, vibrating on its own, this procedure yields reliable results even in the presence of moderate noise. However, while measuring on an integral wheel, the vibration ranges over the whole structure. Thus the measured signals contain coupling and mistuning effects. A method for reliably fitting one or multiple SDOF models to these data is not found to the author's knowledge at the moment of writing this paper.

Of course, Multi-Degree-of-Freedom (MDOF) models will do that job. Reliably fitting an MDOF model to measured data from SG is almost impossible due to the large number of parameters, restriction of results of only a subset of blades, heavy noise, and the usually random character of parameter identification methods.

Artificial Intelligence Algorithms are tested as a new approach without the need for a physical model in the background. Machine learning algorithms based on linear regression are facing their limits since the basic fitting problem mentioned above remains the same. Using an artificial neural network (see Fig. 12) performs better. As a downside, a huge amount of training data is required for a reliable backpropagation to finally obtain damping ratios that are close to their input labels. During the training process, input weights w_j of each neuron (Fig. 13) are simultaneously adapted [23].

Before the triumphant advance of reduced order models due to meaningful inputs from FE models, lumped mass models (Fig. 11) with spring and damper elements were employed to generate synthetic vibrational test data in the sense of a linear MDOF model. Those applications are prone to produce countless resonance crossings in the sense of a Monte-Carlo Simulation with varying but known inputs (mistuning, damping, inter-blade coupling).

In the scope of this paper, approximately 80,000 resonance crossings are generated from one of those lumped mass models. Damping ratios as well as uncoupled and coupled frequencies are randomly distributed within their usual ranges. This training dataset covers relevant cases that may turn up in real data.

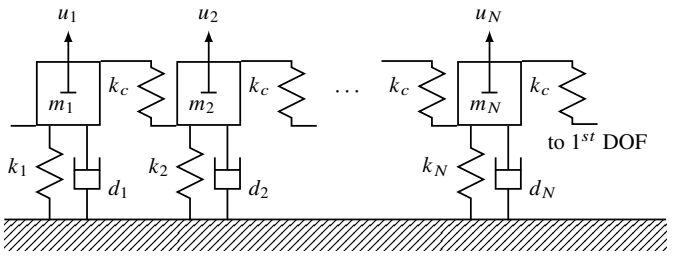

FIGURE 11: CYCLICALLY CLOSED LUMPED MASS MODEL WITH SPRING AND DAMPER ELEMENTS

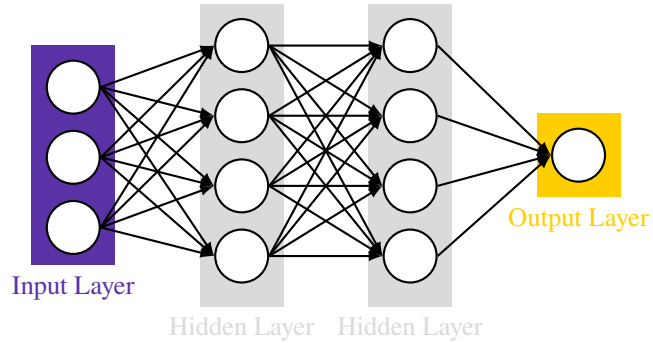

FIGURE 12: SCHEMATIC VISUALIZATION OF A SIMPLE FEED FORWARD NEURONAL NETWORK

Different levels of random noise are added to simulate real measured data.

To obtain a suitable neural network architecture, multiple combinations of different numbers of layers and nodes are investigated. A good network architecture is identified with a single input layer with 501 nodes (the generated or measured data after normalization), two hidden layers with 16 nodes each, and a single output layer with one node (as the damping ratio). An odd number of input layers was chosen with the concept that the resonance's peak is positioned in the middle of the input data range. For the sake of readiness, the visualization of the artificial neural network in Fig. 12 is rather schematic than realistic.

Normalizing the input data (Fig. 14) is crucial to make the trained neural network independent of real amplitudes and eigenfrequencies. The frequencies are normalized so that the frequency at the maximum peak amplitude becomes 1. A normed frequency range of about 0.97 to 1.03 is used to derive 501 input values from the vibrational amplitude. Those amplitudes are normalized in a way that the normalized peak amplitude of each dataset, in the center of the frequency range, equals 1.

Neither normalization affects the damping ratios. Normalization may be thought of as replacing the axes values of a diagram with different values while the shape of the data shown in the diagram remains the same. The damping ratio

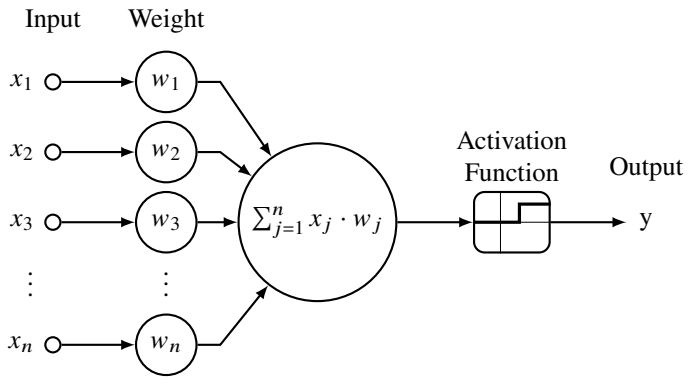

FIGURE 13: SCHEMATIC VISUALIZATION OF AN ARTIFICIAL NEURON

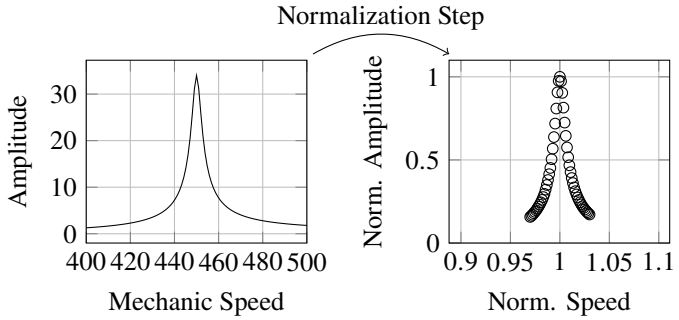

FIGURE 14: NORMALIZATION STEP FROM CONTINUOUSLY MEASURED DATA TO DISCRETE MEASUREMENT POINT

depends only on the shape of the resonance curve.

For implementation, the TensorFlow machine learning package [24, 25] is chosen since it is easily available and can be integrated into existing software. The MDOF algorithm is available in Matlab, therefore also the data handling and normalization tasks are implemented in Matlab. The TensorFlow algorithms turn out to be very efficient. Data generation and training of a comprehensive model took a few minutes on a standard laptop with medium performance.

RESULTS

Figure 15 shows the dynamic stress of blade 5 during the resonance crossing M8 derived from a single BTT plane and two SG positions of that blade. The three trends match quite well with each other. This is remarkable since the analysis of SG and BTT has nothing in common. Consequently, there is a high trust in this measurement result. The resonance trend itself is quite promising for different damping evaluators since the shape of the transfer function equals one of a lumped mass model. However, in the trend of SG 5.2, there is another peak visible roughly 3 rps before the main peak. Also, the BTT signal reveals some additional resonances before and after the resonance peak. Please note that the number of raw data points in the SGs is too high, for the sake of readiness, the scatter plots are smoothed by binning data in small slices. Further, two lines show the SDOF trend (Eq. 7) considering the damping ratio ζ from the neuronal network, maximum stress σ_{res}, and corresponding resonance rotor speed

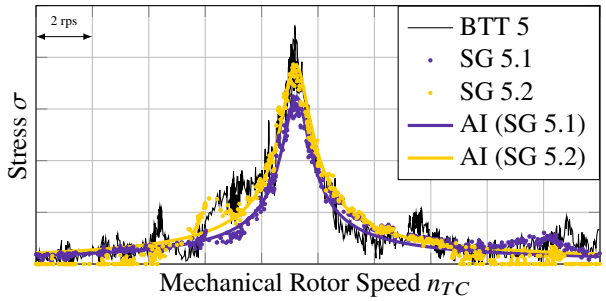

FIGURE 15: VIBRATIONAL STRESS DURING AN M8 RESONANCE CROSSING OF BLADE 5

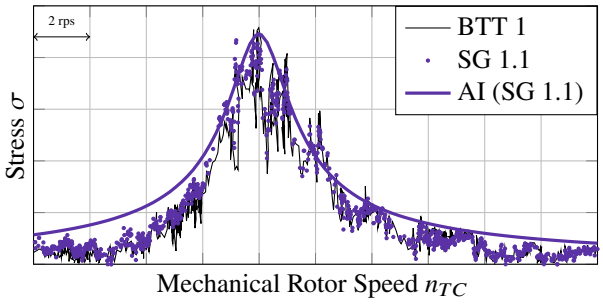

FIGURE 16: VIBRATIONAL STRESS DURING AN M1 RESONANCE CROSSING OF BLADE 1

n_{res}. The SDOF line matches well with both SG data trends.

$$\sigma_{SDOF} = \sqrt{\frac{(2 \cdot \sigma_{res} \cdot \zeta)^2}{\left(1 - \frac{n_{res}}{n_{TC}}^2\right)^2 + \left(2\frac{n_{res}}{n_{TC}}\zeta\right)^2}} \tag{7}$$

Similarly, the resonance crossing of M1 is shown in Fig. 16. SG 1.2 is excluded from this figure since the position (and orientation) is not relevant for the first mode. Please note that this applies also to SG position x.3 in both figures. The agreement between both trends is so good, that it is almost impossible to spot significant deviations between SG 1.1 and BTT of blade 1. Compared to the resonance crossing in Fig. 15, the peak is more massive, one explanation is that the damping ratios of fundamental modes are usually higher (see also Fig. 5). Additionally, there is more than one peak visible. Most probably, this is linked to unavoidable blade mistuning. Thus a single engine order excites more than one resonance within the frequency range of a mode family. Both effects (higher damping and multiple resonances) reinforce the impression of a broad response spectrum. As a consequence, the SDOF trend with the AI-evaluated damping seems to be too high. Most probably this is linked to the assumption of a single resonance, meaning that the maximum amplitude is not the true amplitude of that peak but a superposition of multiple peaks that are not considered by an SDOF shape.

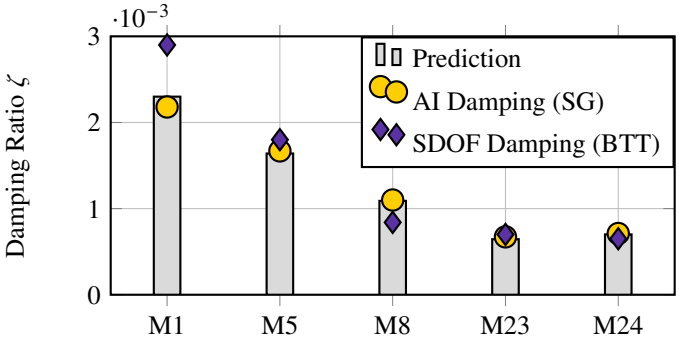

FIGURE 17: COMPARISON OF PREDICTED DAMPING RATIO, AI-BASED EVALUATION ON SG DATA AND SDOF ANALYSIS OF BTT DATA

CONCLUSION

Showcasing the blade vibration measurement results of a radial compressor wheel, this paper uses two state-of-the-art measurement techniques and a modern approach based on a neuronal network to make more out of the available data. Thus, this paper closes a certain gap in validating damping ratios which are predicted based on the concept of acoustic emissions. The findings in this paper may support the next-generation technologies to respond to demands from new applications and fuels.

Unfortunately, the prediction of damping ratios does not include effects from inter-blade coupling (e.g., different nodal diameter forms) and thus is unable to predict damping in the sense of well-known aero-dynamic damping curves. For higher modes, if those curves are rather flat, this drawback may be neglectable. For fundamental modes, the prediction may rather confirm mean damping values.

As an outlook, the damping prediction may be directly used in the design phase of new components or to validate damping ratios from fluid-structure interaction. Regarding the newly introduced AIBVAM, the use case may extend from normalized data in the frequency domain to raw data in the time domain to deliver also amplitude and resonance frequency. Further extension may include BTT data as well. First in the frequency domain after the manual evaluation step. Second, usage of raw data (time of arrival) to save the time-consuming evaluation during the measurement post-processing. Additionally, a reduced order model could be used to support the data generation including physical information in the data set. Using a kind of physically informed training dataset, an inverse parameter identification process should be possible. Then not only a damping ratio is not but also the underlying mistuning pattern or even the resonance's forcing.

ACKNOWLEDGMENTS

The authors would like to express their sincere gratitude to Turbo Systems Switzerland Ltd. for the opportunity to contribute to the future of turbocharger technology. Turbo Systems has provided the necessary equipment to conduct that research. The authors also appreciate the permission to publish this content and share their findings with the scientific community. The authors hope that this work will contribute to the advancement of knowledge and innovation in the field of turbomachinery.

REFERENCES

[1] Mutter, Alexander, Behrendt, Detlef, Domenig, Franco, Ma, Simon, Ruch, David and Senn, Stephan. "Next Generation Axial Turbocharger Fit for a Carbin-Neutral World." 2023. Paper: 057.

[2] Wang, Qiuwen, Zhang, Hu, Huang, Jiabei and Zhang, Pengfei. ""The use of alternative fuels for maritime decarbonization: Special marine environmental risks and solutions from an international law perspective"." *Frontiers in Marine Science* Vol. 9 (2023). DOI 10.3389/fmars.2022.1082453.

[3] Pinto, Valeria, Battiato, Giuseppe and Firrone, Christian Maria. "Reduced Order Models for Bladed

Disks With Contact Mistuning at Blade Root Joints." GT2023-103078. Boston, MA, June 26–30, 2023. DOI 10.1115/GT2023-103078.

[4] Denis, Sophie, Hoffait, Sébastien, Ligot, Jérôme, de Cazenove, Jean and Salles, Loïc. "Improvement and Validation of an Autonomous Experimental System to Identify BLISK Mistuning." GT2023-102903. Boston, MA, June 26–30, 2023. DOI 10.1115/GT2023-102903.

[5] Ligot, Jérôme, Denis, Sophie, Hoffait, Sébastien, de Cazenove, Jean and Golinval, Jean-Claude. "Development of an Acoustic Excitation Test Bench to Support the Validation of Bladed Disks." GT2022-81933. Amsterdam, Nederlands, June 26–30, 2022. DOI 10.

[6] Otobe, T., Iwakami, A. and Filsinger, D. "Blade vibration visualization of dual volute turbine with vaned nozzle by using high speed Digital Image Correlation." *15th International Conference on Turbochargers and Turbocharging*: pp. 251–261. 2023.

[7] Bladh, J. R. "Efficient Predictions of the Vibratory Response of Mistuned Bladed Disks by Reduced Order Modeling." Phd thesis, The University of Michigan. 2001.

[8] Castanier, Matthew P. and Pierre, Christophe. "Modeling and analysis of mistuned bladed disk vibration: current status and emerging directions." *Journal of Propulsion and Power* Vol. 22 No. 2 (2006): pp. 384–396.

[9] Giersch, Thomas, Hönisch, Peter, Beirow, Bernd and Kühhorn, Arnold. "Forced Response Analyses of Mistuned Radial Inflow Turbines." *Journal of Turbomachinery* Vol. 135 No. 3 (2013): p. 031034. DOI 10.1115/1.4007512. URL https://doi.org/10.1115/1.4007512.

[10] Castanier, Matthew and Pierre, Christophe. "Using Intentional Mistuning in the Design of Turbomachinery Rotors." *Aiaa Journal - AIAA J* Vol. 40 (2002): pp. 2077–2086. DOI 10.2514/2.1542.

[11] Beirow, Bernd, Figaschewsky, Felix, Kühhorn, Arnold and Bornhorn, Alfons. "Vibration analysis of an axial turbine blisk with optimized intentional mistuning pattern." *Journal of Sound and Vibration* Vol. 442 (2019): pp. 11–27. DOI 10.1016/j.jsv.2018.10.064.

[12] Nakos, Alex, Beirow, Bernd, Wirsum, Manfred, Markus Schafferus, Marios Sasakaros, Vogt, Damian and Zobel, Arthur. "Mistuning and Damping of a Radial Turbine Wheel. Part 3: Validation of Intentional Mistuning During Machine Operation."

[13] Maywald, Thomas, Backhaus, Thomas, Schrape, Sven and Kühhorn, Arnold. "Geometric Model Update of Blisks and its Experimental Validation for a Wide Frequency Range." GT2017-63446. Charlotte, NC, June 26–30, 2017. DOI 10.

[14] *Automated Meshing Algorithm for Generating As-Manufactured Finite Element Models Directly From As-Measured Fan Blades and Integrally Bladed Disks*. Oslo, Norway, June 11–15. No. GT2018-76375 in *Proceedings of ASME Turbo Expo 2018* (2018). DOI 10.

[15] Yang, M-T and Griffin, JH. "A reduced-order model of mistuning using a subset of nominal system modes." *J. Eng. Gas Turbines Power* Vol. 123 No. 4 (2001): pp. 893–900.

[16] Spengler, Sebastian, Leitenmayer, Christoph, Willeke, Tobias and Aurahs, Lutz. "High Cycle Fatigue - Advanced Development and Design Methods for Increased Robustness." 2023. Paper: 042.

[17] Beirow, B., Maywald, T., Figaschwesky, F., Heinrich, C. R., Kühhorn, A. and Giersch, T. "Simplified Determination of Aerodynamic Damping for Bladed Rotors. Part 1: Experimental Validation at Rest." 2016. Paper: GT2016-56535, https://doi.org/10.1115/GT2016-56535.

[18] Figaschwesky, F., Kühhorn, A., Beirow, B., Giersch, T., Nipkau, J. and Meinl, F. "Simplified Determination of Aerodynamic Damping for Bladed Rotors. Part 2: Experimental Validation during Operation." 2016. Paper: GT2016-56458, https://doi.org/10.1115/GT2016-56458.

[19] Weber, Robby. "Ein Beitrag zur schwingungssicheren Auslegung von radialen Turbomaschinen mit Fokus auf Mistuning und Dämpfung." Dissertation, BTU Cottbus-Senftenberg. 2019.

[20] Nakos, Alex, Schafferus, Markus, Sasakaros, Marios and Zobel, Arthur. "Intentional Mistuning: Forced Response Limitation of Radial Turbines by Means of Intentional Mistuning." Final report. 2023. Hxxxx, not yet published.

[21] Maywald, Thomas, Beirow, Bernd, Heinrich, Christoph R. and Kühhorn, Arnold. "Vacuum Spin Test Series of a Turbine Impeller With Focus on Mistuning and Damping by Comparing Tip Timing and Strain Gauge Results." 2015. Paper: GT2018-76934, https://doi.org/10.1115/GT2015-42649.

[22] Robinson, W. W. and Washburn, R. S. "A Real Time Non-Interference Stress Measurement System (NSMS) for Determining Aero Engine Blade Stresses." 1991. Instrument Society of America pp91-103.

[23] Vapnik, Vladimir N. "An Overview of Statisctical Learning Theory." *IEEE Transactions on Neural Networks* Vol. 10 No. 5 (1999): pp. 988–999. DOI 10.1109/72.788640.

[24] TensorFlowDevelopers. "Tensorflow (v2.15.0)." (2023). DOI 10.5281/zenodo.10126399.

[25] Abadi, Martín, Agarwal, Ashish, Barham, Paul, Brevdo, Eugene, Chen, Zhifeng, Citro, Craig, Corrado, Greg S., Davis, Andy, Dean, Jeffrey, Devin, Matthieu, Ghemawat, Sanjay, Goodfellow, Ian, Harp, Andrew, Irving, Geoffrey, Isard, Michael, Jia, Yangqing, Jozefowicz, Rafal, Kaiser, Lukasz, Kudlur, Manjunath, Levenberg, Josh, Mané, Dandelion, Monga, Rajat, Moore, Sherry, Murray, Derek, Olah, Chris, Schuster, Mike, Shlens, Jonathon, Steiner, Benoit, Sutskever, Ilya, Talwar, Kunal, Tucker, Paul, Vanhoucke, Vincent, Vasudevan, Vijay, Viégas, Fernanda, Vinyals, Oriol, Warden, Pete, Wattenberg, Martin, Wicke, Martin, Yu, Yuan and Zheng, Xiaoqiang. "TensorFlow: Large-Scale Machine Learning on Heterogeneous Systems." (2015). URL https://www.tensorflow.org/. Software available from tensorflow.org.

APPENDIX A. NATURAL MODE SHAPES OF RELEVANT RESONANCE CROSSINGS

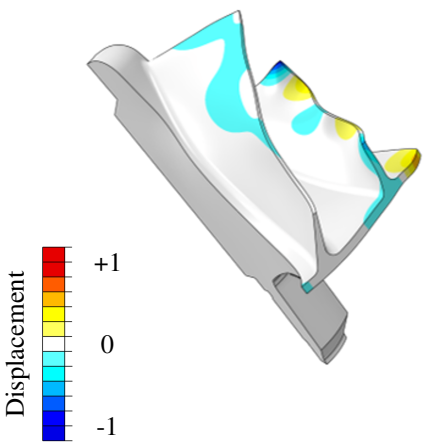

(a) Natural Mode Shape M23

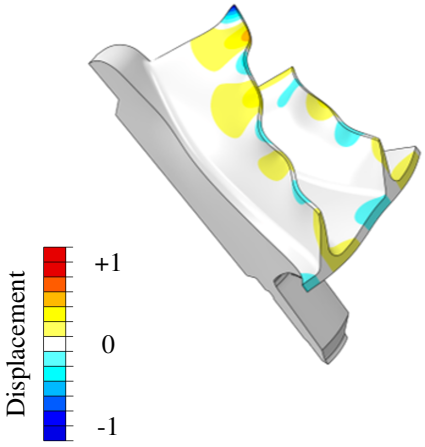

(b) Natural Mode Shape M24

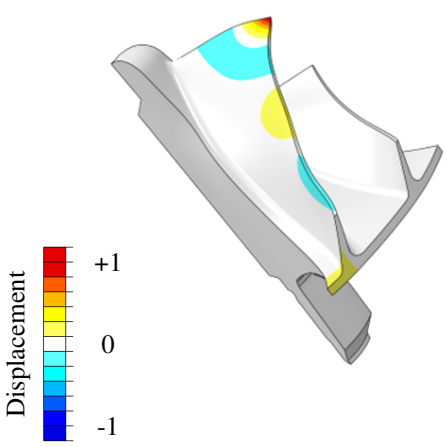

(c) Natural Mode Shape M8

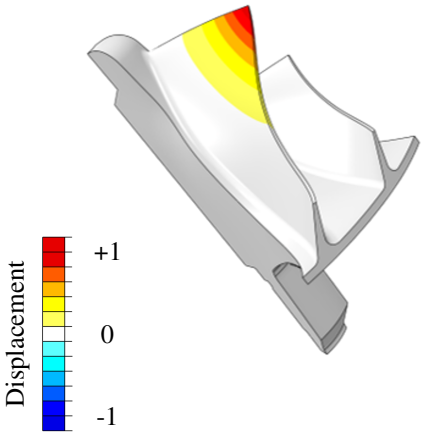

(d) Natural Mode Shape M1

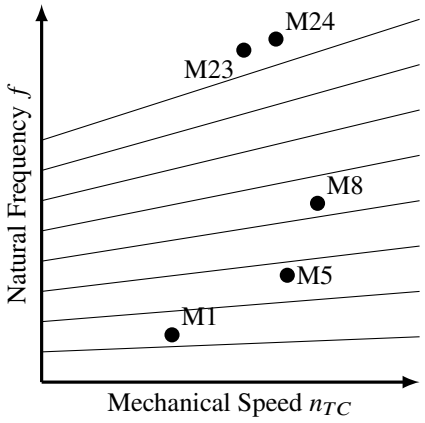

(e) Recall: Schematic Campbell Diagramm

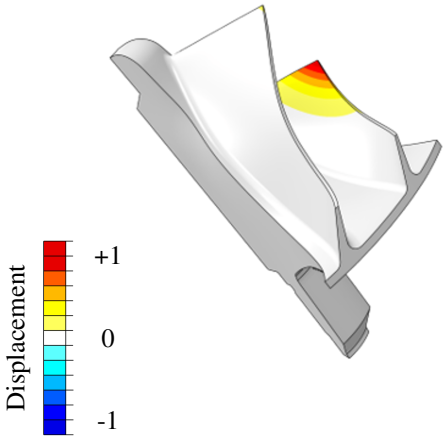

(f) Natural Mode Shape M5

APPENDIX B. RESONANCE CROSSINGS

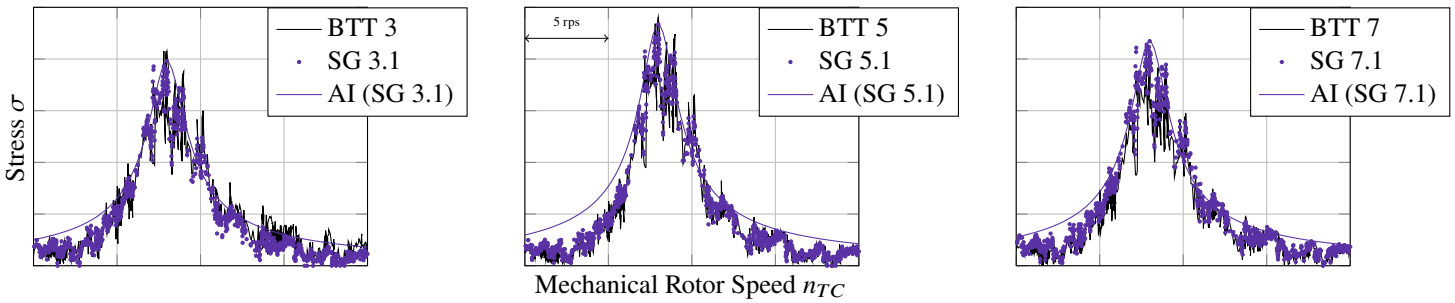

FIGURE 19: RESONANCE CROSSING M1

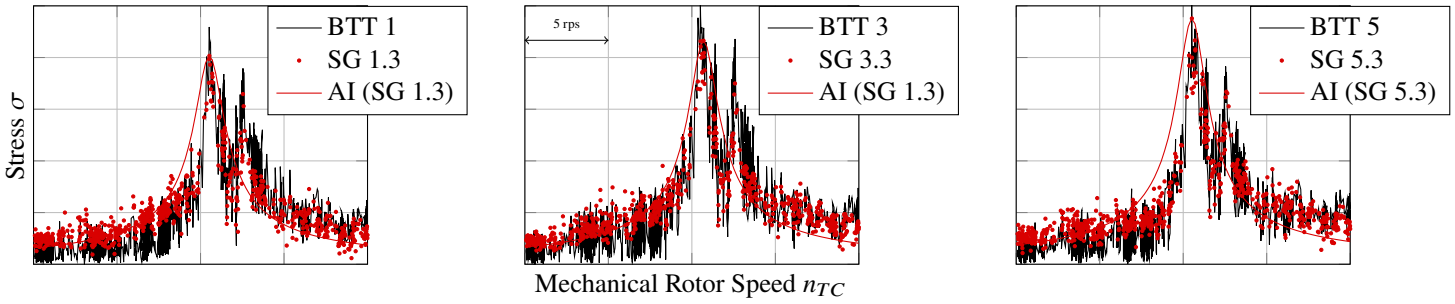

FIGURE 20: RESONANCE CROSSING M5

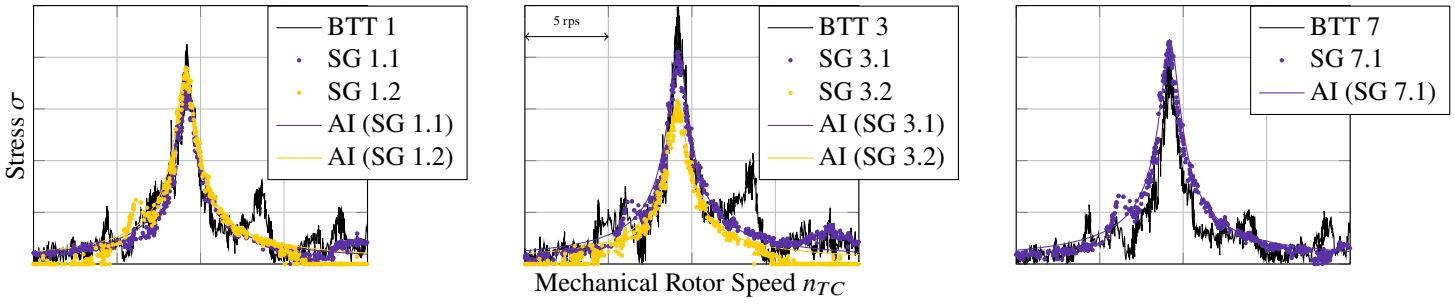

FIGURE 21: RESONANCE CROSSING M8

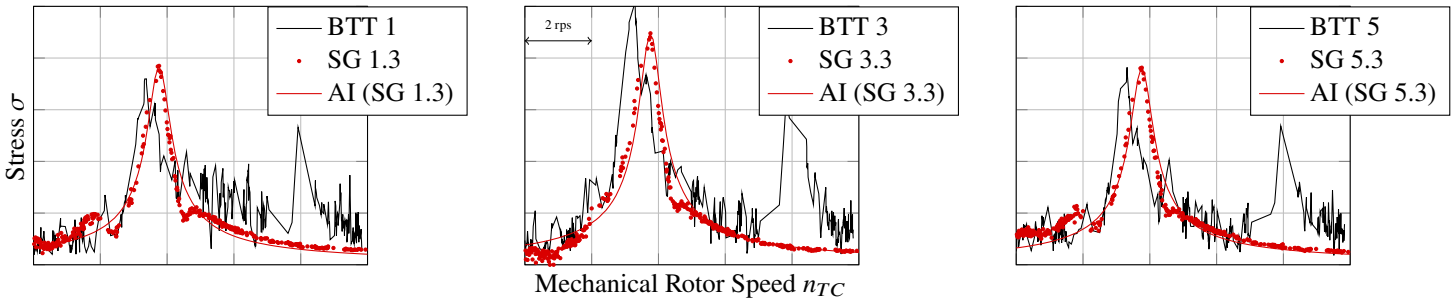

FIGURE 22: RESONANCE CROSSING M23

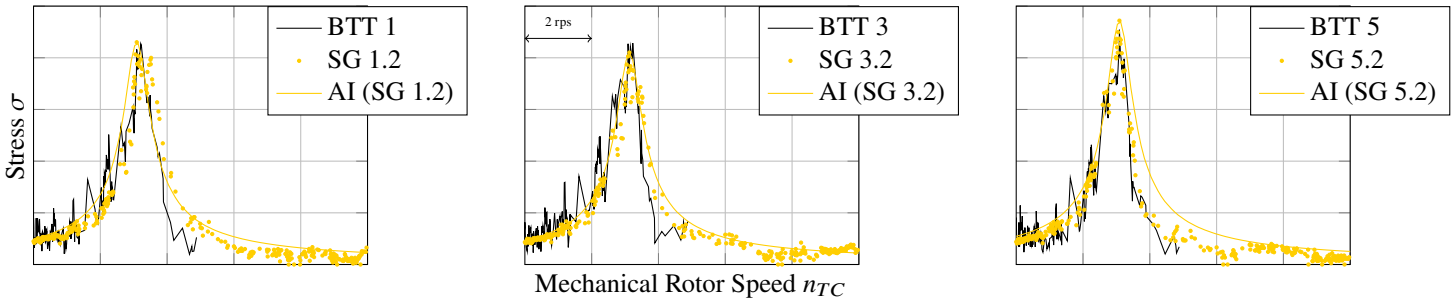

FIGURE 23: RESONANCE CROSSING M24

APPENDIX C. TEST